First-principles prediction of the mechanical properties and electronic structure of ternary aluminum carbide $Zr_3Al_3C_5$

Jingyang Wang,[1,2] Yanchun Zhou,[1] Zhijun Lin,[1,3] Ting Liao,[1,3] and Ling Feng He[1,3]
[1]*Shenyang National Laboratory for Materials Science, Institute of Metal Research, Chinese Academy of Sciences, Shenyang 110016, China*
[2]*International Centre for Materials Physics, Institute of Metal Research, Chinese Academy of Sciences, Shenyang 110016, China*
[3]*Graduate School of Chinese Academy of Sciences, Beijing 100039, China*
(Received 22 June 2005; revised manuscript received 8 February 2006; published 12 April 2006)

In this paper, we predicted the possible mechanical properties and presented the electronic structure of $Zr_3Al_3C_5$ by means of first-principles pseudopotential total energy method. The equation of state, elastic parameters (including the full set of second order elastic coefficients, bulk and shear moduli, Young's moduli, and Poisson's ratio), and ideal tensile and shear strengths are reported and compared with those of the binary compound ZrC. Furthermore, the bond relaxation and bond breaking under tensile and shear deformation from elasticity to structural instability are illustrated. Because shear induced bond breaking occurs inside the NaCl-type ZrC_x slabs, the ternary carbide is expected to have high hardness and strength, which are related to structural instability under shear deformation, similar to the binary carbide. In addition, mechanical properties are interpreted by analyzing the electronic structure and chemical bonding characteristics accompanying deformation paths. Based on the present results, $Zr_3Al_3C_5$ is predicted to be useful as a hard ceramic for high temperature applications.

DOI: 10.1103/PhysRevB.73.134107 PACS number(s): 81.05.Je, 62.20.Dc, 71.20.−b

I. INTRODUCTION

Refractory binary transition metal carbides (TMC), such as TiC, NbC, ZrC, and HfC, are characterized by high hardness, high strength, high melting point, good thermal shock and wear resistance, and chemical inertness. These carbides are widely used in high temperature environments or as hard ceramics.[1] However, poor oxidation resistance and intrinsic brittleness have restricted their applications. Recent developments in synthesizing ternary aluminum carbides by incorporating Al in binary carbides highlight a possible way to solve these problems. It has been reported that ternary titanium aluminum carbide, Ti_3AlC_2, platelets were found to form in Al doped TiC.[2] Prepared under proper conditions, new ternary aluminum carbides have been successfully synthesized in Ti-Al-C, Nb-Al-C, Zr-Al-C, and Hf-Al-C systems, using the binary transition-metal carbides and aluminum as starting materials.[3]

Ternary aluminum carbides in the Ti-Al-C and Nb-Al-C systems, such as Ti_3AlC_2, Ti_2AlC, and Nb_2AlC, have been identified to crystallize with the space group $P6_3/mmc$.[4,5] Microscopic investigations have shown that all of these ternary carbides consist of two alternately stacked structural units. The crystal structures can be described as nanoscale blocks of TiC_x or NbC_x in a NaCl-type structure that is intercalated and mirrored by close-packed Al atomic planes. These ternary aluminum carbides display outstanding properties, such as high damage tolerance, good high temperature oxidation resistance, and intrinsic toughness at room temperature due to their nanolaminated crystal structure.[6] Furthermore, these ternary carbides have high moduli and strength that are desirable for structural materials.

Compounds in the Zr-Al-C system, on the other hand, have different types of crystal structures. Three equilibrium phases, $Zr_2Al_3C_5$, $Zr_3Al_3C_5$ (previously reported with the chemical formula of $ZrAlC_{2-x}$ in Ref. 7), and Zr_5Al_3C, have been reported in the Zr-Al-C system.[5] Among them, $Zr_2Al_3C_5$ and $Zr_3Al_3C_5$ were determined to have the hexagonal symmetry, and Zr_5Al_3C was identified with the Mo_5Si_3-type crystal structure. Compared to the extensively studied Ti-Al-C and Nb-Al-C based ceramics, the properties of ternary Zr-Al-C compounds are much less known. The reasons are attributed to difficulties in synthesizing bulk Zr-Al-C materials.

Recently, the fracture strength and Vickers hardness were primitively characterized for bulk $Zr_2Al_3C_5$ and $ZrAlC_2$ ($Zr_3Al_3C_5$) sintered from $Zr_2Al_3C_5$ and $ZrAlC_2$ powders prepared by the solid-state reaction of ZrC, C, and Al.[8,9] The authors have conducted theoretical studies of the electronic structure, chemical bonding, and equations of state of $Zr_2Al_3C_5$ by means of *ab initio* pseudopotential total energy calculations.[10] $Zr_2Al_3C_5$ was predicted to have interesting properties such as low hardness, easy machinability, damage tolerance, and oxidation resistance based on its nanolaminated structure.[10] Results also showed that $Zr_2Al_3C_5$ might have properties different from the binary carbide, ZrC. It was shown that the intrinsic oxidation resistance of binary carbide, such as TiC, could be greatly improved by making it into ternary carbide that contains Al, such as Ti_3AlC_2.[11] The excellent oxidation resistance resulted from the protective Al_2O_3 scale, which forms in high temperature environments. For ternary Zr-Al-C based compounds, like $Zr_3Al_3C_5$, if continuous ZrO_2 and/or Al_2O_3 scales can form, the material would have good oxidation resistance at high temperatures. Recently, the authors have successfully synthesized $Zr_3Al_3C_5$ powders by means of a pressureless sintering using Zr-Al intermetallics and graphite as starting materials.[12] Tetragonal ZrO_2 and α-Al_2O_3 were identified after $Zr_3Al_3C_5$ powders

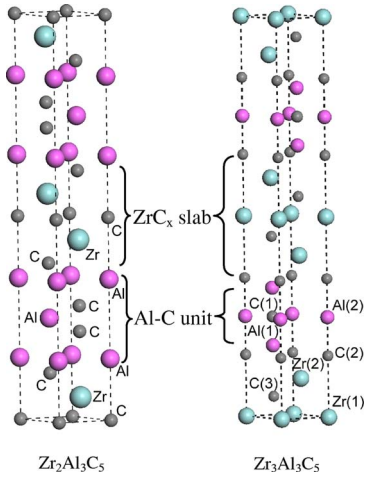

FIG. 1. (Color online) Crystal structures of $Zr_2Al_3C_5$ and $Zr_3Al_3C_5$. The Zr, Al, and C atoms are indexed with numbers according to various coordination environments.

were oxidized in air at temperatures up to 1500 °C. Unfortunately, the oxidation kinetics of bulk $Zr_3Al_3C_5$ is still not fully clarified. Despite these new developments, intrinsic mechanical, physical, and chemical properties are not yet available for $Zr_3Al_3C_5$.

As can be seen from the crystal structures shown in Fig. 1, $Zr_3Al_3C_5$ and $Zr_2Al_3C_5$ have distinguishably different crystal structures. The main difference centers on the atomic configurations linking the ZrC_x slabs. As described by Gesing and Jeitschko,[13] $Zr_3Al_3C_5$ may be viewed as an intergrown structure consisting of two kinds of layers.[13] One is the nonstoichiometric ZrC_x slab in a NaCl-type structure and the other consists of Al and C atoms in an arrangement similar to that of the binary aluminum carbide, Al_4C_3. The nonstoichiometric ZrC_x slabs in $Zr_2Al_3C_5$, however, are linked by different Al-C units. Although both materials contain ZrC_x slabs, the mechanical properties of $Zr_3Al_3C_5$ may be different from those of $Zr_2Al_3C_5$, because of the different interplanar adhesive strength linking the ZrC_x slabs. Therefore, it is necessary to clarify how the mechanical properties of such a material are determined by their intergrown structure of ZrC_x slabs and Al_4C_3-type Al-C layers. Because of this crystallographic arrangement, it is of particular interest to investigate the mechanical properties and chemical bonding characteristics of $Zr_3Al_3C_5$. In this study, we computed the equation of state (EOS), elastic moduli, ideal strengths, electronic structure, and chemical bonding characteristics of $Zr_3Al_3C_5$ using the first-principles computational scheme. The investigation aims to predict possible mechanical properties, and further, to show the relationship between the electronic structure and the mechanical properties.

The remainder of this paper is organized as follows. The computational details are described in Sec. II. In Sec. III, we present our results for equilibrium geometry and electronic structure characteristics. The EOS, elastic stiffness, the full set of elastic coefficients, and mechanical parameters are reported in Sec. IV. The ideal stress-strain relationship, ideal tensile and shear strength, together with the processes of bond relaxation and bond breaking for material strained from elasticity to structural instability, are illustrated in Sec. V. Finally, the concluding remarks are given in Sec. VI.

II. COMPUTATIONAL DETAILS

The CASTEP code was used in the present calculations,[14] wherein the Vanderbilt-type ultrasoft pseudopotential[15] and generalized gradient approximation[16] (GGA-PW91) were employed. The plane-wave basis set cutoff was 450 eV for all calculations. The special points sampling integration over the Brillouin zone was employed by using the Monkhorst-Pack method with a $10\times10\times2$ special k-points mesh.[17] To investigate the ground state electronic structure and EOS, the equilibrium crystal structures were optimized at various isotropic hydrostatic pressures ranging from 0 to 50 GPa. Lattice parameters, including lattice constants and internal atomic coordinates, were modified independently to minimize the enthalpy and interatomic forces. The Broyden-Fletcher-Goldfarb-Shanno (BFGS) minimization scheme[18] was used in geometry optimization. The tolerances for geometry optimization are difference on total energy within 5×10^{-6} eV/atom, maximum ionic Hellmann-Feynman force within 0.01 eV/Å, maximum ionic displacement within 5×10^{-4} Å and maximum stress within 0.02 GPa. We have shown that the present first-principles calculation scheme is reliable on predicting crystal structure, elastic stiffness, and interatomic force constants of ternary transition metal carbides.[19–21]

The calculations of projected density of states were performed using a projection of the plane-wave electronic states onto a localized linear combination of atomic orbitals (LCAO) basis set. In the present calculation, the LCAO basis set was the atomic pseudo-orbitals corresponding to the closed valence shell containing the valence electrons. The numbers of pseudo-orbitals were chosen as 4 for C, 4 for Al, and 9 for Zr. The s,p valence orbitals of C, as well as the s, p orbitals of Al and the s, p, and d orbitals of Zr were included in the calculation of partial density of states (PDOS). Since $Zr_3Al_3C_5$ is a metallic system, partial occupancies were introduced to eliminate discontinuous changes in the total energy, which were created when energy bands crossed the Fermi level during self-consistent electronic minimization. Twelve additional empty bands were included in the electronic minimization, and we used the Gaussian smearing scheme with a smearing width of 0.1 eV.

The elastic coefficients were determined from a first-principles calculation by applying a set of given homogeneous deformations with a finite value and calculating the resulting stress with respect to optimizing the internal degrees of freedoms, as implemented by Milman *et al.*[22] The criteria for convergence in optimizing atomic internal freedoms were selected as follows: difference on total energy within 1×10^{-6} eV/atom, ionic Hellmann-Feynman forces within 0.002 eV/Å and maximum ionic displacement within 1×10^{-4} Å. Two strain patterns, one with nonzero ε_{11} and ε_{23} components and the other with a nonzero ε_{33}, generated stresses related to all five independent elastic coefficients for a unit cell with a hexagonal symmetry. Three positive and three negative amplitudes were applied for each strain com-

TABLE I. Theoretical and experimental crystal symmetry, lattice constants a and c (in Å), c/a ratio, free internal atomic parameters z (atom) of $Zr_3Al_3C_5$, as well as the bulk modulus B (in GPa) and its pressure derivative B' derived from the equation of state.

Method	Symmetry	a	c	c/a	z (atom)	B	B'
Calc.	$P6_3/mmc$	3.316	27.387	8.259	z(C1)=0.0502	205	3.8
					z(C2)=0.2498		
					z(C3)=0.1535		
					z(Al1)=0.1777		
					z(Al2)=0.2497		
					z(Zr1)=0.5960		
Expt.[a]	$P6_3mc$	3.343	27.609	8.259	z(C1)=0.0510		
					z(C2)=0.2511		
					z(C3)=0.1508		
					z(Al1)=0.1776		
					z(Al2)=0.2448		
					z(Zr1)=0.5955		

[a]Reference 13.

ponent with the maximum strain value of 0.5%. We determined the elastic stiffness from a linear fit of the calculated stress as a function of strain. The compliance tensor S was calculated as the inverse of the stiffness tensor, $S=C^{-1}$. Other mechanical parameters, such as the bulk modulus, Young's moduli, and Poisson's ratio were calculated from the compliance tensor. The shear modulus was calculated according to the Voigt approximation.[23]

Deformation and failure modes of $Zr_3Al_3C_5$ lattice are studied. To obtain the ideal stress-strain relationships, we employed a method widely used to study the ideal strength and lattice stability of metals and ceramics.[24–27] By deforming the crystal from its elastic state to structural instability, the stress-strain curves are computed for $\langle 0001\rangle(0001)$ uniaxial tension and $\langle 1\bar{2}10\rangle(0001)$ shear deformation (a possible easy slip system for hexagonal compound with large c/a ratio). For the tensile deformation, a series of incremental tensile strains were applied to the crystal. To ensure that the material was under an uniaxial stress state, relaxation of the structure perpendicular to the applied strain direction was performed by holding the applied strain fixed and adjusting the other two normal strain components independently until the calculated conjugate Hellmann-Feynman stresses were both less than 0.2 GPa. For the $\langle 1\bar{2}10\rangle(0001)$ shear deformation path, the crystal was relaxed until all of the stresses orthogonal to the applied stress are reduced to less than 0.2 GPa. These computations produce the stress versus strain curves for both the tensile and shear deformations. The first-reached maximum in these curves is the ideal strength of the material under a particular strain path, provided that no other instability occurs before it. For comparison, the stress-strain curves for ZrC were also computed for the $(001)\langle 001\rangle$ tension and $(110)\langle\bar{1}10\rangle$ shear deformation (the primary slip system for the NaCl-type transition metal carbide at low temperature).[28]

III. EQUILIBRIUM GEOMETRY AND ELECTRONIC STRUCTURE

To compute the equilibrium crystal structure of $Zr_3Al_3C_5$, we optimized the previously reported crystal structure[13] by relaxing the cell degrees of freedom with constrained space group $P6_3mc$. Then, we analyzed the space group of a fully relaxed unit cell. It shows that $Zr_3Al_3C_5$ belongs to the space group $P6_3/mmc$ within a precision of 0.005 Å by performing symmetry operations. For the initial structure with space group $P6_3mc$, the Al(2) atoms were located off the center of the trigonal bipyramid formed by C(1) and C(2) atoms. In the present computation, the Al(2) atoms locate on a mirror plane on the center of the trigonal bipyramid, which yields to a higher symmetry space group $P6_3/mmc$. Very recently, Lin *et al.* have confirmed the space group $P6_3/mmc$ for $Zr_3Al_3C_5$ in experiments by means of selected area electron diffraction and convergent beam electron diffraction methods.[29] Theoretical lattice parameters are listed in Table I, together with the experimental values for comparison. The computed lattice constants a and c are consistent with experimental data within 1% deviation. Furthermore, the two sets of internal atomic parameters, z, also have close values. The theoretical density is 5.280 g/cm^3 and it agrees well with the experimental value found in the JCPDS data file (card no. 32-0030), 5.282 g/cm^3. Therefore, the present first-principles computation is able to reliably reproduce the equilibrium crystal structure of $Zr_3Al_3C_5$.

To better understand the nature of the interatomic bonding, the electronic structure was examined. Figure 2 shows the total and projected density of states (PDOS) of $Zr_3Al_3C_5$. The lowest lying states from −14.39 to −8.78 eV originate mainly from the C 2s orbitals with slight contributions from Al-p and Zr-d orbitals. The p-p and p-d covalent bonding dominate the states ranging from −7.38 eV to the Fermi level. From −7.38 to −3.77 eV, the p-p and s-p bonding states come from C-Al interatomic bonds. We compared the

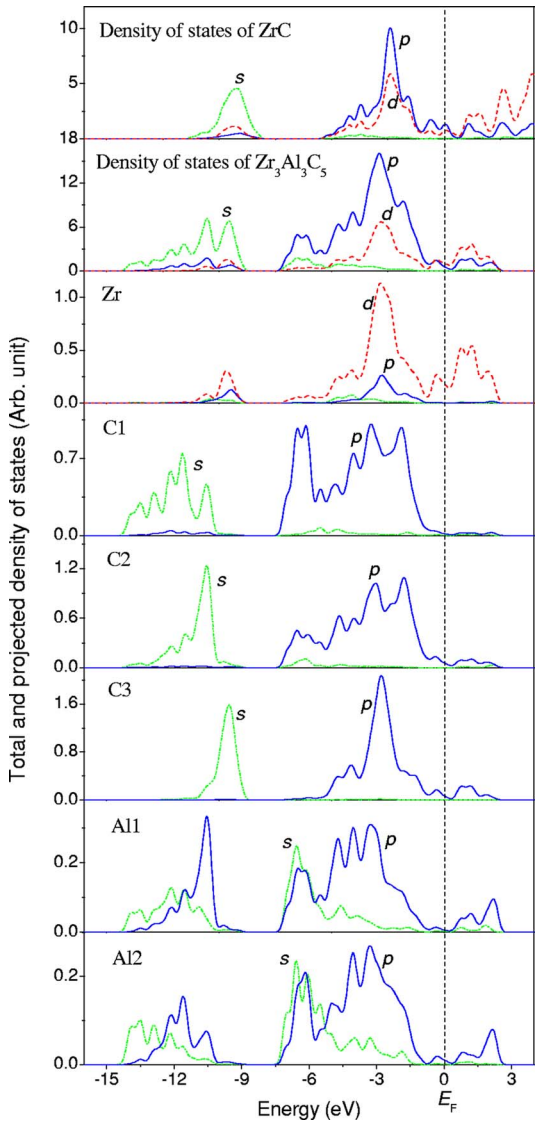

FIG. 2. (Color online) Total and projected electronic density of states of ZrC and $Zr_3Al_3C_5$.

Zr d t_{2g}−C p σ-like bonds in ZrC and $Zr_3Al_3C_5$, and found that the characteristics of Zr-C bonds are rather similar in the two carbides. The C $2p$−Zr $4d$ bonding peak is located at around −2.88 eV away from the Fermi level in $Zr_3Al_3C_5$, which is similar to the corresponding peak at around −2.40 eV in ZrC. In addition, the bond lengths of Zr-C are 2.289 Å, 2.360 Å, and 2.480 Å in $Zr_3Al_3C_5$, and 2.345 Å in ZrC. Therefore, the strong Zr-C bonds are well preserved in the ternary carbide. It should be noted that the bond length of Zr2-C2 (2.480 Å) is about 8.34% and 5.08% longer than that of Zr1-C3 (2.360 Å) and Zr2-C3 (2.289 Å), respectively. This implies that the Zr2-C2 bond may be weaker than other Zr-C bonds in $Zr_3Al_3C_5$.

The bonding peak located at around −1.83 eV corresponds to the Al $3p$−C $2p$ covalent bonds. These hybridization states are located at a higher energy range than the Zr $4d$−C $2p$ bonding states. Therefore, the chemical strength of certain Al-C bond is weaker than that of the Zr-C covalent bonds. There are two types of Al-C bonds in $Zr_3Al_3C_5$ according to different atomic arrangements. Identifying the character of these Al-C bonds is very important to predict the mechanical properties of $Zr_3Al_3C_5$, because variations of these bonding strengths will lead to distinctly different performances. If the Al1-C2 is weaker than the Al1-C1 bond, $Zr_3Al_3C_5$ could be regarded as a combination of ZrC_x slabs and Al-C blocks with a Al_4C_3 structure. On the other hand, if the Al1-C2 is stronger than the Al1-C1 bond, $Zr_3Al_3C_5$ could be described as covalently bonded Zr-C-Al blocks being interleaved by close-packed Al-C atomic planes. Unfortunately, strengths of the Al1-C1 and Al1-C2 bonds could not be obtained from the PDOS figures, due to an extensive energy range of the p-derived states. To quantitatively analyze the adhesions of Al-C bonds, the adhesive energies were calculated by cleaving the Al1-C2 and Al1-C1 bonds parallel to the basal plane.

The energy of breaking the Al1-C2 bonds $E_{adhesive}^{\text{Al1-C2}}$ was computed by

$$E_{adhesive}^{\text{Al1-C2}} = E_{total}^{Zr_3C_4\otimes} + E_{total}^{\otimes Al_3C} - E_{total}^{Zr_3Al_3C_5}, \quad (1)$$

where $E_{total}^{Zr_3C_4\otimes}$ is the total energy of $Zr_3C_4\otimes$ blocks after eliminating Al_3C blocks from the unit cell, $E_{total}^{\otimes Al_3C}$ is the total energy of Al_3C blocks after eliminating the $Zr_3C_4\otimes$ blocks from the unit cell and $E_{total}^{Zr_3Al_3C_5}$ is the total energy of $Zr_3Al_3C_5$. In the same way, the adhesive energy of breaking the Al1-C1 bonds $E_{adhesive}^{\text{Al1-C1}}$ was computed by

$$E_{adhesive}^{\text{Al1-C1}} = E_{total}^{Zr_3C_4Al_2\otimes} + E_{total}^{\otimes AlC} - E_{total}^{Zr_3Al_3C_5}, \quad (2)$$

where the $E_{total}^{Zr_3C_4Al_2\otimes}$ is the total energy of $Zr_3C_4Al_2\otimes$ blocks after eliminating AlC atomic planes from the unit cell, $E_{total}^{\otimes AlC}$ is the total energy of Al-C atomic plane after eliminating $Zr_3C_4Al_2\otimes$ blocks from the unit cell and $E_{total}^{Zr_3Al_3C_5}$ is the total energy of $Zr_3Al_3C_5$.

The computed adhesive energies yield 1.18 eV/atom and 0.41 eV/atom by breaking the Al1-C2 and Al1-C1 bonds, respectively. Therefore, the adhesion strength of the Al1-C1 bond is much weaker than that of the Al1-C2 bond. We further calculated the adhesive energy of Zr2-C2 bond, which is the longest Zr-C bond in $Zr_3Al_3C_5$. The result yields 0.92 eV/atom, which is located between that of the Al1-C1 and Al1-C2 bonds. The bonding strength results suggest that, at the equilibrium crystal structure, $Zr_3Al_3C_5$ could be described as strong covalently bonded Al-C-Zr-C-Zr-C-Zr-C-Al blocks interleaved by close-packed Al-C atomic planes. In addition, the Al-C adhesion between those covalent-bonded atomic chains and Al-C planes are relatively weak.

To illustrate the bonding characteristics, Fig. 3 shows the charge density distribution for a slice of the $(11\bar{2}0)$ plane in a $2\times2\times1$ supercell. Figure 3 obviously shows strong covalent bonding within the Al-C-Zr-C-Zr-C-Zr-C-Al atomic blocks (abbreviated as $Zr_3C_4Al_2\otimes$). The adjacent $Zr_3C_4Al_2\otimes$ blocks are interleaved and mirrored by Al-C atomic planes. The electronic density is relatively low in the region between $Zr_3C_4Al_2\otimes$ and Al-C units, which leads to weaker interplanar adhesion.

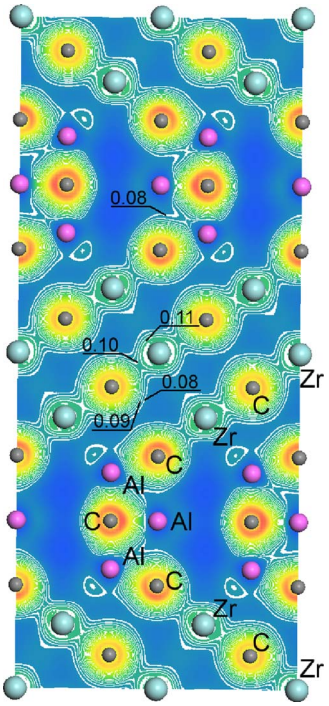

FIG. 3. (Color online) Valence electron density of a slice of the $(11\bar{2}0)$ plane in a $2\times2\times1$ supercell. The white contour lines range from 0.08 to 0.27 electrons/Å^3.

IV. EQUATION OF STATE AND ELASTIC STIFFNESS

Figure 4 plots the relative unit cell volume, V/V_0, as a function of external pressure. By fitting the data with the Birch-Murnaghan equation,[30] bulk modulus B_0 and its pressure derivative B_0' are obtained to be 205 GPa and 3.8, respectively. The bulk modulus of $Zr_3Al_3C_5$ is comparable to that of ZrC (229 GPa), computed within the same first-principles scheme. The B_0 of $Zr_3Al_3C_5$ is definitely higher than that of $Zr_2Al_3C_5$, which has a value of only 160 GPa.[10] In Fig. 5, we present the pressure dependence of lattice constants a and c and display changes of the axial ratio, c/a, in the inset. The c/a ratio decreases almost linearly with increasing hydrostatic pressure continuously to ~25 GPa, and then it decreases less rapidly at higher pressures. The trend in c/a versus pressure demonstrates that c contracts more dramatically than a in the pressure range examined. Therefore,

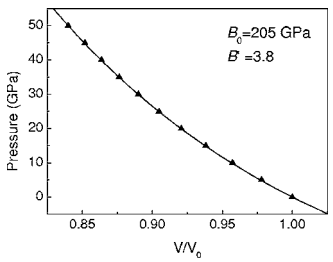

FIG. 4. Relative unit cell volume V/V_0 as a function of external hydrostatic pressure. The bulk modulus B_0 and its pressure derivative B_0' are determined to be 205 GPa and 3.8, respectively, by fitting the data with the Birch-Murnaghan equation.

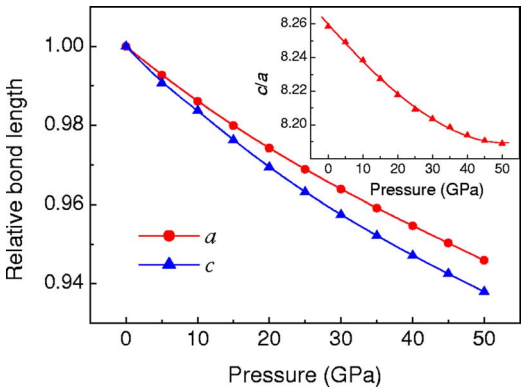

FIG. 5. (Color online) Pressure dependence of lattice constants a and c. The inset shows the c/a ratio versus pressure.

the material is stiffer in the basal plane than in c when $Zr_3Al_3C_5$ is under isotropic pressure. This elastic anisotropy suggests that interplanar bonding along c is weaker than intraplanar bonding along the basal plane in $Zr_3Al_3C_5$.

Anisotropic elasticity has been investigated for Ti_3SiC_2 at various pressures both by experiment[31] and by first-principles calculation.[32] In these studies, the strength of interatomic bonding was characterized by its resistance against external pressure. The Ti-Si and Ti-C bonds shrank by 8% and 5%, respectively, when hydrostatic pressure increased from 0 to 50 GPa. Combined with electronic structure analysis, the interplanar Ti-Si covalent bond was found to be weaker than the Ti-C bonds in $TiC_{0.67}$ blocks. This difference in bond strength led to the mechanical anisotropy of Ti_3SiC_2. Following the same method to evaluate the strengths of interatomic bonding against pressure for $Zr_3Al_3C_5$, we examine the degree of bond length contraction under various pressures, and illustrate the results in Fig. 6. The lowest lying curve is seen to be associated with the Al1-C1 bond, which is the most compressible. Above it are the curves for Zr2-C2, Al1-C2, Zr2-C3, and Al2-C1 covalent bonds, and these bonds show similar compressibility with increasing applied pressure. The least compressible among these is the Zr2-C3 bond. Figure 6 indicates that the Al1-C1 bonding is softer than other interatomic bonds, such as Zr2-C2 and Al1-C2 bonds, in $Zr_3Al_3C_5$ under hydrostatic pressure.

The elastic stiffness of a crystal determines its response to an applied strain (or stress) near equilibrium and provides

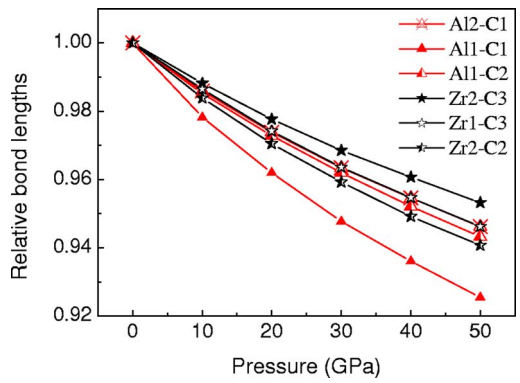

FIG. 6. (Color online) Relative bond-length contractions at various pressures.

TABLE II. Computed second order elastic coefficients c_{ij} (in GPa) of ZrC and $Zr_3Al_3C_5$, together with experimental values of ZrC for comparison.

	Method	c_{11}	c_{12}	c_{44}	c_{33}	c_{13}	c_{66}
ZrC	Calc.	455	116	152			
	Expt.[a]	472	99	159			
$Zr_3Al_3C_5$	Calc.	429	110	179	378	93	160

[a]Reference 33.

information about bonding characteristics. To our best knowledge, the elastic moduli of $Zr_3Al_3C_5$ have not been reported. In Table II, we include the computed full set of second order elastic coefficients of $Zr_3Al_3C_5$, together with the theoretical and experimental values of ZrC for comparison.[33] The theoretical data agree well with experimental values of ZrC. It is also noted that $Zr_3Al_3C_5$ and ZrC have similar elastic coefficients. For example, the moduli representing stiffness against uniaxial strains, c_{11} and c_{33} of $Zr_3Al_3C_5$, are about 94% and 83%, respectively, of c_{11} of ZrC. The c_{44} and c_{66} of $Zr_3Al_3C_5$, which correspond to the resistance against $\{100\}\langle 110\rangle$ and $\{010\}\langle 001\rangle$ shear deformations, are about 1.18 and 1.05 times, respectively, of c_{44} of ZrC.

Table III presents the computed mechanical parameters of $Zr_3Al_3C_5$, such as bulk modulus B, shear modulus G, anisotropic Young's moduli E, and Poisson's ratio, together with theoretical and experimental values of ZrC.[33] The magnitudes of the mechanical parameters of $Zr_3Al_3C_5$ are rather similar to those of ZrC, varying within 10%. This implies that the complex ternary aluminum carbide $Zr_3Al_3C_5$ has comparable elastic stiffness to the binary carbide ZrC.

V. BOND-BREAKING AND IDEAL STRENGTHS

Material deformation is strain dependent and elastic parameters may not always give accurate account for all macroscopic mechanical properties, such as hardness. The reason can be attributed to the fact that these elastic parameters are computed under equilibrium conditions; while material deformation associated with experimentally obtained strengths occurs at a specific range of strains where bonding characteristics change significantly. Therefore, studies of the stress-strain relationships following a material strained from elasticity to the limit of its structural stability and the underlying bond-responding processes are useful in understanding its experimental strengths and hardness at ambient conditions.

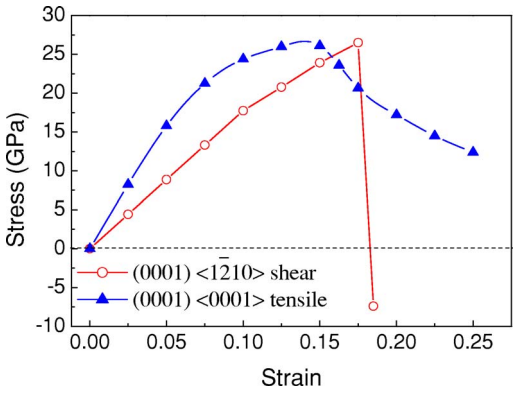

FIG. 7. (Color online) Ideal stress-strain curves of tensile and shear deformation for $Zr_3Al_3C_5$.

In Fig. 7, we present the calculated stress-strain curves for $Zr_3Al_3C_5$. Several interesting features are noticed for the $\langle 1\bar{2}10\rangle(0001)$ shear path: (i) stress increases with strain almost linearly before the material reaches structural instability; (ii) shear stress drops abruptly after a critical strain; (iii) there is no obvious "yielding" when the compound passes from elasticity to structural instability. On the other hand, for the $(0001)\langle 0001\rangle$ tension: (i) breakdown of elasticity occurs long before the strain reaches a critical bond-breaking point; (ii) there is an obvious "yielding" that follows a gradual reduction of the tensile stress after its maximum value. In the following discussions, we will show that these features originate from the softening and breaking of Al-C and Zr-C bonds that are involved in different deformation modes.

To understand the trend in the stress-strain curve for shear deformation, we examined the bond-relaxation processes at various strains. Figure 8 shows the valence charge density distribution on the $(11\bar{2}0)$ atomic plane in $Zr_3Al_3C_5$ at various shear strains. It shows that all bonds accommodate strain almost homogeneously, and no local bond softening occurs before the critical strain, as seen in Fig. 8(a) for $\varepsilon=0.05$. Both the Al-C and Zr-C bonds remain strong up to the bond-breaking point. Of the most interest, breaking of the Zr2-C2 bond, instead of the weakest Al1-C1 bond, is responsible for the structural instability of $Zr_3Al_3C_5$ under shear deformation as shown in Fig. 8(b) for $\varepsilon=0.175$. Because failure of this material occurs inside the NaCl-type ZrC_x slabs, it is likely that the binary and ternary carbides will show similar me-

TABLE III. Computed bulk modulus B, shear modulus G, anisotropic Young's moduli E, and Poisson's ratio υ of ZrC and $Zr_3Al_3C_5$, together with experimental values of ZrC polycrystalline for comparison.

	Method	B (GPa)	G (GPa)	E (GPa)	υ
ZrC.	Cal.	229	170	408	$\upsilon_{xy}=0.21$
	Expt.[a]	223	170	407	$\upsilon_{xy}=0.19$
$Zr_3Al_3C_5$	Calc.	202	166	$E_x=388$	$\upsilon_{xy}=0.22$
				$E_z=346$	$\upsilon_{xz}=0.19$
					$\upsilon_{zx}=0.17$

[a]Reference 33.

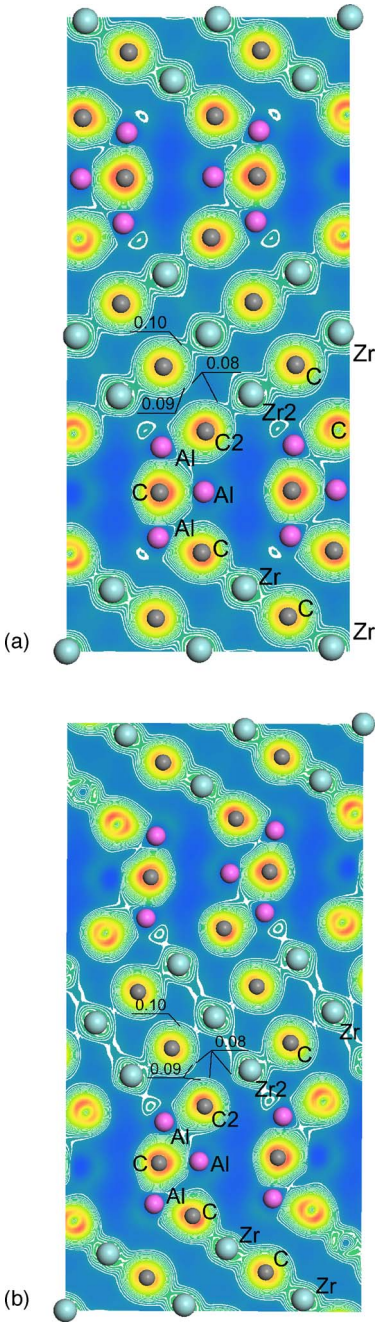

FIG. 8. (Color online) Valence electron density of a slice of the $(11\bar{2}0)$ plane in a $2\times2\times1$ supercell under shear deformations of (a) $\varepsilon=0.05$, and (b) $\varepsilon=0.175$. Obviously, the shear-induced structural instability occurs by breaking the Zr2-C2 bonds in the ZrC_x slab.

chanical properties that are determined by shear-induced structural instability.

When we focus on the valence charge density distributing on the $(11\bar{2}0)$ atomic plane in $Zr_3Al_3C_5$ under tension, a different bond-relaxation mechanism is observed. As shown in Fig. 9, the softening and breaking of the weakest Al1-C1 bonds is now responsible for the failure of $Zr_3Al_3C_5$. In contrast to Al-C bonds being stable under shear deformation, the Al1-C1 bond softens considerably under tensile strains long

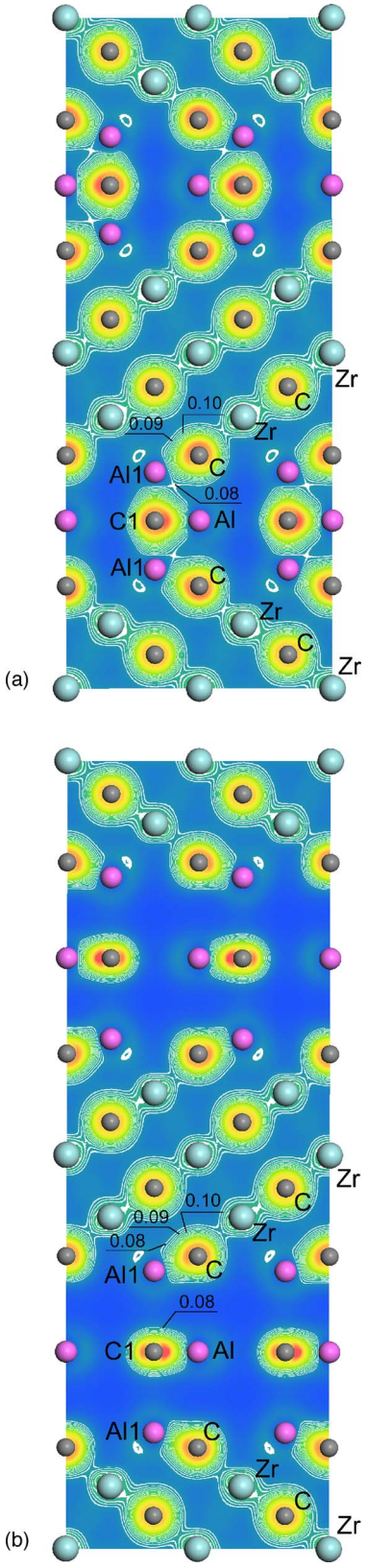

FIG. 9. (Color online) Valence electron density of a slice of the $(11\bar{2}0)$ plane in a $2\times2\times1$ supercell under tensile deformations of (a) $\varepsilon=0.05$, and (b) $\varepsilon=0.25$. $Zr_3Al_3C_5$ is seen to cleave by breaking the Al1-C1 bonds.

before bond breaking. The bond length of Al1-C1 elongates 6%, 17%, 32%, 57%, and 78% under tensile strains of 0.05, 0.10, 0.15, 0.20, and 0.25, respectively. This produces the notable "yielding" in the stress-strain curve shown in Fig. 7. When the tensile stress increases, the Al1-C1 bond does not abruptly experience a bond-breaking event, because of the delocalized nature and spatial extension of its *p-p* hybridization. Therefore, "yielding" occurs, which follows a gradual reduction of the tensile stress under increased tensile strains. On the other hand, the Zr-C bonds in the NaCl-type ZrC_x slabs remain stable during tensile deformation along the *c* direction.

From the computed stress-strain curves, the ideal shear and tensile strengths are 26.5 GPa and 26.8 GPa, respectively. These values lead to a shear-to-tensile strength ratio of about 1. For the binary carbide, ZrC, we compounded the ideal shear and tensile strengths, which yield 29 GPa and 31 GPa, respectively. The presented ideal shear strength of ZrC, 29 GPa, is comparable to some transition metal carbides TiC, TiN, and HfC, which were reported as 35, 31, and 30 GPa, respectively, by Jhi *et al.*[24] The strengths of $Zr_3Al_3C_5$ are, therefore, comparable with those of ZrC, and they represent the upper limit of stresses attainable prior to failure. Again, comparison on these ideal strengths indicates that $Zr_3Al_3C_5$ may have similar mechanical properties to ZrC.

Generally speaking, hardness reflects the resistance of a material against permanent plastic deformation. The mechanism for plastic deformation involves the nucleation and movement of dislocations. The mobility of dislocation could be estimated from the Peierls stress or the stress required moving a dislocation one atomic Burgers vector. For strongly covalent materials, like binary transition metal carbides, the very low mobility of dislocation kinks is the rate-determining factor for dislocation motion and is in turn determined by the very high bond-breaking energy under a large shear strain.[34–36] With the help of calculated mechanical parameters, we estimate the maximum value of Peierls shear stress to initiate the movement of a dislocation in its glide plane for $Zr_3Al_3C_5$ by[37]

$$\sigma_S = \frac{2G}{1-\nu}\exp\left(-\frac{2\pi\lambda}{b}\right) \tag{3}$$

where $\lambda = 3-2\nu/4(1-\nu)d$, G is the shear modulus, b the Burgers vector, d the spacing between atomic slip plans, and ν the Poisson's ratio.

Following Krenn *et al.*,[38] we use d by $1/6\langle 111\rangle$ and b by $1/2\langle 110\rangle$ for ZrC with NaCl-type structure. Computed from the lattice constant (4.691 Å) of ZrC, d is 1.354 Å and b is 3.317 Å. Because slip in $Zr_3Al_3C_5$ occurs by breaking the Zr2-C2 bonds, the interplanar distance between Zr2-C2 atomic planes is used as d to calculate its Peierls stress. Therefore, d is set as 1.576 Å and b is the lattice constant along the basal plane (3.316 Å); ν for both carbides is taken as 0.19. Results from Eq. (3) can be used to compare the relative maximum magnitude of Peierls stress between binary and ternary carbides. The calculated σ_S for $Zr_3Al_3C_5$ reaches 78% of the binary carbide. Therefore, similar to ZrC, the ternary carbide, $Zr_3Al_3C_5$, is expected to show very low dislocation mobility. Suggested by the present investigations, experimental hardness of $Zr_3Al_3C_5$ is determined by the response of strong Zr-C covalent bonds to shear strain, and is expected to display a high magnitude.

VI. CONCLUDING REMARKS

In summary, we investigated the equilibrium crystal structure, EOS, elastic moduli, ideal strengths, bond-breaking processes, and electronic structure of $Zr_3Al_3C_5$ by first-principles calculations. The results show how interatomic bonds in this complex ternary carbide respond to applied strains, especially under strains near a critical point of structural instability. We show that the Al-C and Zr-C bonds dominate tensile and shear failures of $Zr_3Al_3C_5$, respectively. The material cleaves by breaking the weakest Al-C bond, while slip plane movement occurs by abruptly breaking the Zr-C bonds under shear strains. Shear induced bond-breaking occurs inside the NaCl-type ZrC_x slabs, which provides $Zr_3Al_3C_5$ to have high shear strength and moduli similar to ZrC. Obtained ideal tensile and shear strengths of this ternary carbide are comparable to its binary counterpart, ZrC. Furthermore, Peierls stresses of the two carbides are compared, and the result shows that dislocation mobility will be low in the two compounds. Results led to a suggestion that $Zr_3Al_3C_5$ has a great potential to be used as a hard ceramic for high temperature applications and should be extensively studied in the future.

ACKNOWLEDGMENT

This work was supported by the National Outstanding Young Scientist Foundation for Y. C. Zhou under Grant No. 59925208, Natural Sciences Foundation of China under Grant Nos. 50232040, 90403027, and 50302011.

[1] H. Nowotny and S. Windisch, Annu. Rev. Mater. Sci. **3**, 171 (1973).
[2] R. Yu, L. L. He, and H. Q. Ye, Acta Mater. **51**, 2477 (2003).
[3] J. C. Schuster, H. Nowotny, and C. Vaccaro, J. Solid State Chem. **32**, 213 (1980).
[4] M. A. Pietzka and J. C. Schuster, J. Phase Equilib. **15**, 392 (1994).
[5] J. C. Schuster and H. Nowotny, Z. Metallkd. **71**, 341 (1980).
[6] M. W. Barsoum, Prog. Solid State Chem. **28**, 201 (2000).
[7] S. I. Mikhalenko, Y. B. Kuz'ma, V. E. Popov, V. N. Gurin, and A. P. Nechitailov, Izv. Akad. Nauk SSSR, Neorg. Mater. **15**, 1948 (1979).
[8] U. Leela-adisorn, S. M. Choi, S. Hashimoto, S. Honda, and H. Awaji, in Proceedings of the 21st International Korea-Japan

Seminar on Ceramics (2004), p. 339.
[9] U. Leela-Adisorn, S. M. Choi, N. Tera, T. Takeuchi, S. Hashimoto, S. Honda, H. Awaji, K. Hayakawa, and A. Yamaguchi, J. Ceram. Soc. Jpn. **113**, 188 (2005).
[10] J. Y. Wang, Y. C. Zhou, Z. J. Lin, and T. Liao, Phys. Rev. B **72**, 052102 (2005).
[11] X. H. Wang and Y. C. Zhou, Corros. Sci. **45**, 891 (2003).
[12] L. F. He, Y. C. Zhou, Y. W. Bao, J. Y. Wang, and M. S. Li (unpublished).
[13] T. M. Gesing and W. Jeitschko, J. Solid State Chem. **140**, 396 (1998).
[14] M. D. Segall, P. L. D. Lindan, M. J. Probert, C. J. Pickard, P. J. Hasnip, S. J. Clark, and M. C. Payne, J. Phys.: Condens. Matter **14**, 2717 (2002).
[15] D. Vanderbilt, Phys. Rev. B **41**, R7892 (1990).
[16] J. P. Perdew, J. A. Chevary, S. H. Vosko, K. A. Jackson, M. R. Pederson, D. J. Singh, and C. Fiolhais, Phys. Rev. B **46**, 6671 (1992).
[17] H. J. Monkhorst and J. D. Pack, Phys. Rev. B **16**, 1748 (1977).
[18] B. G. Pfrommer, M. Côté, S. G. Louie, and M. L. Cohen, J. Comp. Physiol. **131**, 233 (1997).
[19] J. Y. Wang and Y. C. Zhou, Phys. Rev. B **69**, 144108 (2004).
[20] J. Y. Wang and Y. C. Zhou, Phys. Rev. B **69**, 214111 (2004).
[21] J. Y. Wang, Y. C. Zhou, Z. J. Lin, F. L. Meng, and F. Li, Appl. Phys. Lett. **86**, 101902 (2005).
[22] V. Milman and M. C. Warren, J. Phys.: Condens. Matter **13**, 241 (2001).
[23] P. Ravindran, L. Fast, P. A. Korzhavyi, B. Johansson, J. Wills, and O. Eriksson, J. Appl. Phys. **84**, 4891 (1998).
[24] S.-H. Jhi, S. G. Louie, M. L. Cohen, and J. W. Morris, Jr., Phys. Rev. Lett. **87**, 075503 (2001).
[25] R. H. Telling, C. J. Pickard, M. C. Payne, and J. E. Field, Phys. Rev. Lett. **84**, 5160 (2000).
[26] S. Ogata, J. Li, and S. Yip, Science **298**, 807 (2002).
[27] Y. Zhang, H. Sun, and C. F. Chen, Phys. Rev. Lett. **93**, 195504 (2004).
[28] L. E. Toth, in *Transition Metal Carbides and Nitrides* (Academic Press, New York, 1971).
[29] Z. J. Lin, M. J. Zhuo, L. F. He, Y. C. Zhou, M. S. Li, and J. Y. Wang, Acta Mater. (to be published).
[30] F. Birch, J. Geophys. Res. **83**, 1257 (1978).
[31] A. Onondera, H. Hirano, T. Yuasa, N. F. Gao, and Y. Miyamoto, Appl. Phys. Lett. **74**, 3782 (1999).
[32] J. Y. Wang and Y. C. Zhou, J. Phys.: Condens. Matter **15**, 1983 (2003).
[33] D. J. Green, in *An Introduction to the Mechanical Properties of Ceramics* (Press Syndicate of the University of Cambridge, Cambridge, 1998).
[34] S.-H. Jhi, J. Ihm, S. G. Louie, and M. L. Cohen, Nature (London) **399**, 132 (1999).
[35] J. J. Gilman, Science **261**, 1436 (1993).
[36] J. J. Gilman, Mater. Sci. Eng. A **209**, 74 (1996).
[37] A. M. Kosevich, "Crystal dislocations and the theory of elasticity," in *Dislocations in Solids*, edited by F. R. N. Nabarro (North-Holland Publishing Company, Amsterdam, 1979).
[38] C. R. Krenn, J. W. Morris, Jr., S.-H. Jhi, and J. Ihm, Relationships between atomistic bonding and intrinsic macroscopic hardness," in *Hard Coatings Based on Borides, Carbides & Nitrides*, edited by A. Kumar, Y.-W. Chung, and R. W. J. Chia (TMS, 1998).